AFRL-IF-RS-TR-2006-166
Final Technical Report
May 2006

THREE-DIMENSIONAL NANOBIOCOMPUTING ARCHITECTURES WITH ℵ-HYPERCELLS: REVOLUTIONARY SUPER-HIGH-PERFORMANCE COMPUTING PLATFORM

Microsystems and Nanotechnologies

APPROVED FOR PUBLIC RELEASE; DISTRIBUTION UNLIMITED.

AIR FORCE RESEARCH LABORATORY
INFORMATION DIRECTORATE
ROME RESEARCH SITE
ROME, NEW YORK

STINFO FINAL REPORT

This report has been reviewed by the Air Force Research Laboratory, Information Directorate, Public Affairs Office (IFOIPA) and is releasable to the National Technical Information Service (NTIS). At NTIS it will be releasable to the general public, including foreign nations.

AFRL-IF-RS-TR-2006-166 has been reviewed and is approved for publication

APPROVED: /s/

THOMAS E. RENZ
Project Engineer

FOR THE DIRECTOR: /s/

JAMES A. COLLINS
Deputy Chief, Advanced Computing Division
Information Directorate

REPORT DOCUMENTATION PAGE

Form Approved
OMB No. 074-0188

1. AGENCY USE ONLY (Leave blank)	2. REPORT DATE	3. REPORT TYPE AND DATES COVERED
	MAY 2006	Final Dec 2004 – Dec 2005

4. TITLE AND SUBTITLE
Three-Dimensional Nanobiocomputing Architectures With ℵ-Hypercells: Revolutionary Super-High-Performance Computing Platform

5. FUNDING NUMBERS
C - FA8750-05-C-0024
PE - 61101E
PR - NGBQ
TA - 10
WU - 01

6. AUTHOR(S)
Sergey Lyshevski, Vlad Shmerko, Svetlana Yanushkevich, Marina Lyshevski

7. PERFORMING ORGANIZATION NAME(S) AND ADDRESS(ES)
Microsystems and Nanotechnologies
70 Angels Path
Webster New York 14580

8. PERFORMING ORGANIZATION REPORT NUMBER
N/A

9. SPONSORING / MONITORING AGENCY NAME(S) AND ADDRESS(ES)
Air Force Research Laboratory/IFTC
525 Brooks Road
Rome New York 13441-4505

10. SPONSORING / MONITORING AGENCY REPORT NUMBER
AFRL-IF-RS-TR-2006-166

11. SUPPLEMENTARY NOTES

AFRL Project Engineer: Thomas E. Renz/IFTC/(315) 330-3423 Thomas.Renz@rl.af.mil

12a. DISTRIBUTION / AVAILABILITY STATEENT
APPROVED FOR PUBLIC RELEASE; DISTRIBUTION UNLIMITED.

12b. DISTRIBUTION CODE

13. ABSTRACT *(Maximum 200 Words)*

Microsystems and Nanotechnologies developed a revolutionary 3D3 (Hardware–Software–Nanotechnology) technology to design three-dimensional (3D) nanobiocomputing architectures and Integrated Circuits (ICs). Our technology was based on the design of 3D computing architectures utilizing a three-fold solution: (1) innovative hardware (device/module/system-level and 3D ICs); (2) novel software - Computer Aided Design (CAD) supported by new synthesis and design methods and; (3) enabling nanotechnology. The solution and innovations developed ensure information processing preeminence and computing superiority. We departed from conventional planar IC design (VLSI, ULSI and postULSI) and von Neumann architectures. Novel technologies of massive parallel distributed (pipelined due to systolic processing) computing and information processing in 3D were utilized using devised neuronal-hypercells (ℵ-hypercells) that result in 3D topologies, organizations and architectures. In general, ℵ-hypercells significantly increased the number of bits of information processed and exchanged to compute complex switching functions. Novel highly-efficient synthesis taxonomy and design concepts were developed and demonstrated. The design was accomplished utilizing linear decision diagrams and linear systolic arrays. We integrated fundamental and applied research within innovative computing and molecular electronics technologies, developing representative CAD and sound proof-of-concept software tools.

14. SUBJECT TERMS
Nanotechnology, Molecular Computing, Terascale Architectures

15. NUMBER OF PAGES
34

16. PRICE CODE

17. SECURITY CLASSIFICATION OF REPORT	18. SECURITY CLASSIFICATION OF THIS PAGE	19. SECURITY CLASSIFICATION OF ABSTRACT	20. LIMITATION OF ABSTRACT
UNCLASSIFIED	UNCLASSIFIED	UNCLASSIFIED	UL

TABLE OF CONTENTS

List of Figures

List of Tables

Summary

Under USAF contract, *Microsystems and Nanotechnologies* performed research and technology development in three-dimensional (3D) nanobiocomputing architectures. The major accomplishments are:

1. A novel design concept for Integrated Circuits (ICs) and computing architectures in 3D space was developed and demonstrated. The proposed design is supported by novel software and envisioned hardware technologies. For complex ICs, we performed the design by utilizing neuronal hypercells (ℵ-hypercells) within a neuronal aggregated network. At the system level, benchmarking ICs (that have been widely used to evaluate and assess 2D Very Large Scale Integration / Ultra Large Scale Integration, VLSI/ULSI, design) were examined as proof-of-concept 3D ICs for the envisioned biomolecular computing architectures.
2. Neuronal hypercells that perform complex logics were designed. The aggregated ℵ-hypercells form neuronal 3D ℵ-hypertopologies, thereby implementing nanobiocomputing architectures. Interconnected functional multi-terminal biomolecules form molecular gates (^{M}gates) that comprise 3D ℵ-hypercells.
3. Representative Compute Aided Design (CAD) components were developed to coherently support the reported design tasks for 3D ICs.
4. A DNA transistor (DNA^{T}), as a possible proof-of-concept three-terminal hybrid bioelectronic device, was modeled, simulated and analyzed.

We departed from the two-dimensional (2D) paradigm and 2D topology/organization/architecture of ICs by developing a novel technology that utilizes a three-fold innovative solution:

- hardware (novel 3D molecular devices, ℵ-hypercells, modules and systems);
- software (technology-specific CAD supported by new synthesis and design methods);
- nanotechnology.

Thus, in general, we propose a revolutionary $3D^{3}$ $^{(Hardware–Software–Nanotechnology)}$ technology that ensures super-high-performance computing and information processing. We focused on development of a feasible, practical, affordable and superior technology for massive parallel distributed computing and information processing. The proposed technology will allow one to perform design coherently integrating synthesis tasks at the device/gate and system levels. We depart from conventional 2D VLSI and Complimentary Metal Oxide Semiconductor (CMOS) paradigms. A novel $3D^{3}$ technology will offer:

1 Enormous military advantages because newly designed super-high-performance platforms will guarantee information processing preeminence, computing superiority and memory supremacy;
2 Very strong commercial potential with immediate applications in design of new generations of preeminent processors and memories;
3 Sound technology transfer feasibility to future Air Force systems.

1. Introduction

This contract started December 27, 2004. The overall objective was to devise, design and demonstrate novel super-high-performance three-dimensional (3D) nanobiocomputing architectures with aggregated 3D neuronal-hypercells (ℵ-hypercells) that integrate interconnected functional multi-terminal electronic nanobiodevices (biomolecules). The specific objectives were to:

1 Devise and demonstrate 3D nanobiocomputing architectures designed utilizing a network of aggregated ℵ-hypercells (modeling, analysis and software development) that form ICs.
2 Design ℵ-hypercells that perform complex logics. Develop a library of basic ℵ-hypercells.
3 Develop representative components of 3D nanobiocomputing CAD with a focus on ℵ-hypercells.
4 Design 8-bit arithmetic logic unit (ALU) as a proof-of-concept platform to prove and demonstrate super-high-performance computing capabilities of 3D computing architectures.
5 Model and analyze DNA-based transistors (DNA^T). Examine the electronic properties of biomolecules as electronic nanobiodevices (modeling, simulation and software developments).
6 Analyze the system- and device-level integration, aggregation, compliance and compatibility.

The research at the system and device level was focused on the solution of a number of major problems. The technology developments were concentrated on the following four major tasks:

1. Devise and demonstrate a novel 3D super-high-performance nanobiocomputing architecture utilizing ℵ-hypercells. Developing the unified bottom-up and top-down design taxonomy, aggregate 3D ℵ-hypercells within 3D ℵ-hypertopologies. Design, demonstrate, analyze and evaluate a proof-of-concept ALU.
2. Design and Integrate ℵ-hypercells that perform complex logic. Develop a library of basic ℵ-hypercells for 3D computing architectures. The major problems to be addressed are: synthesis and logic design, as well as ℵ-hypercell aggregation.
3. Develop representative components of 3D nanobiocomputing CAD with a focus on 3D ICs comprised from ℵ-hypercells that integrate functional multi-terminal electronic nanobiodevices. Solve the following problems: (1) logic design and analysis; (2) topology synthesis and aggregation; (3) steady-state and dynamic analysis of DNA^T.
4. Develop high-fidelity and compact (tractable) mathematical models for DNA^T examining electronic properties. These models must support heterogeneous simulations and data-intensive analysis of electronic nanobiodevices aggregated in ℵ-hypercells. Verify models using the experimental data for the electron transport in DNA^T.

For the aforementioned major tasks, in order to accomplish the overall and specific objectives, *Microsystems and Nanotechnologies* successfully accomplished the following:

For Task 1. We devised and demonstrated novel 3D nanobiocomputing architectures utilizing ℵ-hypercells by designing 3D ICs. The synthesis is performed using the unified bottom-up and top-down design taxonomy aggregating 3D ℵ-hypertopologies. This task is supported with programs developed in the C and MATLAB environments. Demonstration, analysis and evaluation are performed for a proof-of-concept ALU and other ICs.

For Task 2. We designed ℵ-hypercells that perform complex logic. We developed a library of basic ℵ-hypercells within nanobiocomputing architectures and 3D ℵ-hypertopologies.

For Task 3. We developed representative components of 3D nanobiocomputing CAD (representative CAD tools) with a focus on design of 3D ICs comprised from ℵ-hypercells. We coherently supported the basic and applied research developing MATLAB- and C-based software.

For Task 4. We modeled, simulated, analyzed and assessed DNA^T as an electronic nanobiodevice for ℵ-hypercells.

2. Methods, Assumptions, and Procedures

Proposed Solution (Methods) – Our proposed solution and technology are based on the design of 3D computing architectures and ICs utilizing a three-fold solution (method):

1. innovative hardware (device/module/system levels and 3D ICs),
2. novel software (CAD supported by new synthesis and design methods),
3. nanotechnology-centered hardware-software co-design.

In particular, *Microsystems and Nanotechnologies* proposed and demonstrated a revolutionary $3D^{3\ (Hardware–Software–Nanotechnology)}$ technology. Our solution ensures information processing preeminence and computing superiority. By introducing the proposed $3D^3$ computing technology, we depart from conventional planar ICs topologies as well as IC design techniques, such as VLSI, ULSI and post ULSI.

A technology of massively parallel distributed (pipelined due to systolic processing) computing and information processing in 3D is utilized using devised ℵ-hypercells. In general, ℵ-hypercells significantly increase the number of bits of information processed and exchanged to compute complex switching functions. The redundancy and parallelism ensures robust fault-tolerant computing. The logic design and mappings are simplified due to the linear decision diagram and linear systolic array for information processing and manipulation. We integrated fundamental and applied research within innovative computing and molecular electronics technologies.

3. Results and Discussions

3. 1. DESIGN TAXONOMY AND LOGIC DESIGN OF THREE-DIMENSIONAL ICS

3. 1. 1. Synthesis Taxonomy

To design novel nanobiocomputing architectures, we utilized an innovative unified top-down and bottom-up synthesis taxonomy. The proposed taxonomy utilized an *x*-design flow map as reported in Figure 1.a. At the system and device levels, the core design themes were integrated within the following four domains:

- Devising (synthesis) with validation;
- Design – optimization;
- Modeling – analysis – evaluation;
- Nanotechnology – fabrication.

A top-down synthesis was performed in the proposed 3D super-large-scale integration (SLSI) design in order to synthesize 3D nanobiocomputing platforms implemented by aggregating $\aleph$-hypercells within ICs. These $\aleph$-hypercells were formed from molecular gates (^{M}gates) as illustrated in Figure 1.b. The bottom-up synthesis was focused on biomolecular electronic devices aggregated as functional molecules that comprise ^{M}gates forming $\aleph$-hypercells. A unified top-down and bottom-up synthesis taxonomy was utilized.

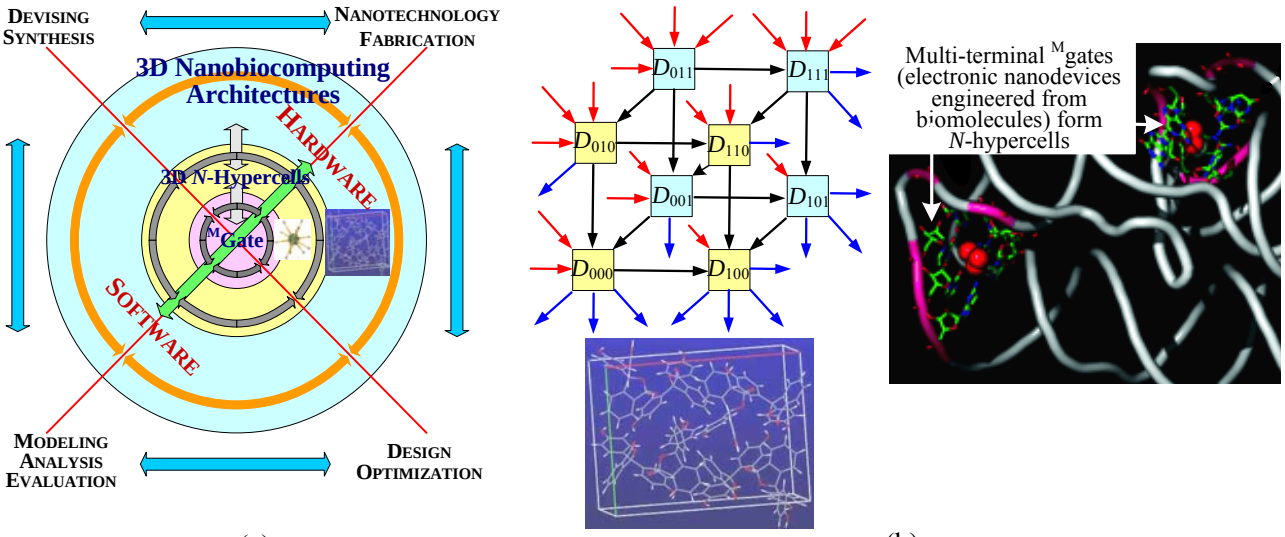

Figure 1. a) *X*-design flow map;
b) $\aleph$-hypercells D_{ijk} formed utilizing multi-terminal ^{M}gates comprised from molecular complexes

Figure 2 reports the major tasks within the top-down and bottom-up syntheses that were concurrently supported by the envisioned CAD to perform SLSI.

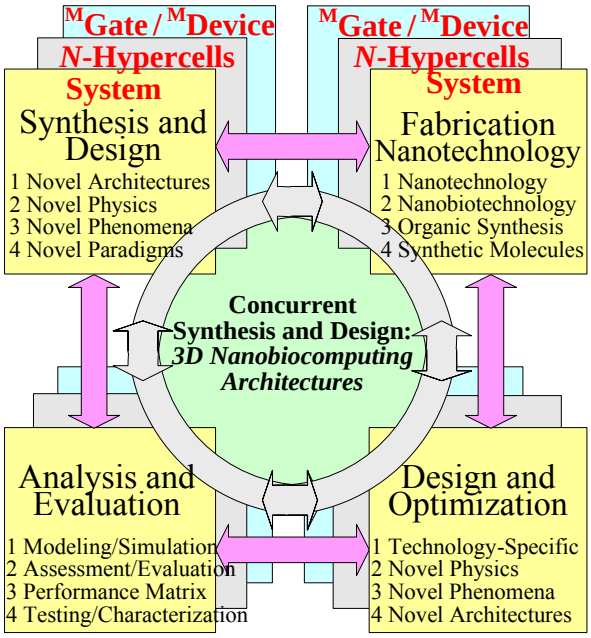

Figure 2. Nanobiocomputing architectures and associated design tasks

The *neuroarchitectronics* paradigm serves as the basis for the design of novel super-high-performance biomolecular computing platforms which can be implemented by utilizing biomolecular 3D ICs. Synthesis, analysis and design of combinational biocomputing hardware are performed with the design of 3D ICs. Using a conventional neuroscience viewpoint, we prototype a neuron as a biomolecular electronic module, while networked neuronal aggregates are prototyped by $\aleph$-hypercell aggregates. The $\aleph$-hypercell aggregates perform processing and computing. Figure 3 documents the proposed 3D nanobiocomputing architecture. The problem is to concurrently design 3D ICs.

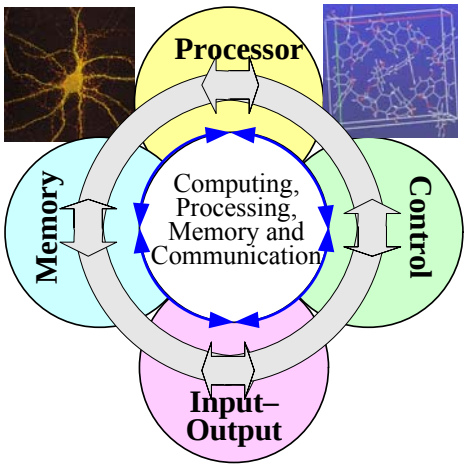

Figure 3. Nanobiocomputing architecture

3. 1. 2. Design of 3D ICs: Data Structure, Decision Diagram, and Hypercells

An innovative solution to perform the system-level logic design for 3D ICs has been found by the *Microsystems and Nanotechnologies* team as reported in this section. We departed from 2D logic design (VLSI, ULSI and postULSI) as well as IC topologies reported in [1]. In general, the proposed SLSI technology mimics highly hierarchical 3D neuronal bio processing platforms (brain). Our fundamental and technological solutions prototype the system architecture, topology and organization observed in nature. This sound solution reflects the envisioned device-level outlook and fabrication technologies. Sections 3.2 and 3.4 introduce and examine possible molecular electronic devices to implement ℵ-hypercells. Three dimensional architectures/organizations/topologies and 3D molecular electronics, unified by the developed 3D design concept, lead to a need for novel CAD developments. The CAD solution, as reported in section 3.3, should be reusable and technology-dependent. The use of 3D ℵ-hypercells, covered in section 3.2, as baseline primitives to design computing platforms, results in a technology-relevant solution. Our solution offers a great deal of adaptability from the design and fabrication technology viewpoints ensuring a coherent correspondence with bioelectronics at the device and system levels

For 2D CMOS ICs, the decision diagram (unique canonical structure) is derived as a reduced decision tree by using topological operators. In contrast, for 3D ICs, a new class of decision diagrams and synthesis methods must be developed. We developed a novel linear decision diagram that is mapped by 3D ℵ-hypercells. The hypercell (cube, pyramid, hexagonal or other 3D topological clusters) is a unique canonical structure which provides a reduced decision tree. These hypercells are synthesized by using topological operators (deleting and splitting nodes). We analyze optimal and suboptimal (technology-specific) topology mappings of complex switching functions. The major optimization criteria are: (1) minimization of decision diagram nodes and circuit terminals; (2) simplification of topological structures (proposed linear arithmetic, versus nonlinear arithmetic, leads to simple synthesis and straightforward embedding of linear decision diagrams into 3D topologies); (3) minimization of path length in decision diagrams; (4) simplification of routing and verification tasks. The reported advantages result in power dissipation reduction, evaluation simplicity, testability enhancement, as well as other important features. For example, the switching power is not only a function of devices/gates/switches (bipolar junction transistors and field-effect transistors, BJTs and FETs, for CMOS), but also a function of circuit topology, design methods, routing, dynamics, switching activities and other factors that can be optimized. We have developed a novel CAD-supported design technology that allows one to design high-performance nanobiocomputing architectures. The proposed methods and technology, concurrently supported by software, allow one to:

1. Synthesize and aggregate ℵ-hypercells thereby designing 3D nanobiocomputing architectures;
2. Perform logic design utilizing novel representations of data structures;
3. Devise and verify a new binary decision diagram synthesis concept;
4. Initiate the developments of representative CAD tools to concurrently support logic design.

The proposed concept will result in SLSI that utilizes a coherent top-down/bottom-up synthesis taxonomy and *nanoarchitectronics*. Novel 3D nanobioarchitecture hardware is envisioned to be implemented as aggregated ℵ-hypercells as the fabrication technologies (molecular electronics) reach technical and technological maturity, economical feasibility and technology acceptance. A number of promising innovative paradigms have been explored in conventional microelectronics [1] and emerging nanoelectronics [2-7]. Addressing the need for fundamental development at the system and device levels,

we examine: (1) design complexity (current CAD-supported methods do not allow one to design ICs with a number of gates more than 1,000,000); (2) device functionality (quantum phenomena must be utilized in molecular complexes which are fabricated using nanotechnology).

The binary decision diagrams (BDD) for representing Boolean functions are used [8]. Reduced-order and optimized BDDs ensure large-scale data manipulations and are used to perform the logic design and circuitry mapping utilizing hardware description languages [9, 10]. The design scheme is

Function (Circuit) ↔ BDD Model ↔ Realization.

The dimension of a decision diagram (number of nodes) is a function of the number of variables and the variables ordering. In general, the design complexity is $\boldsymbol{O(n^3)}$. This complexity significantly limits the design capabilities in terms of ICs complexity (number of gates) for which the design can be performed. The commonly utilized word-level decision diagrams further increase the complexity due to processing of data in word-level format. Therefore, novel concepts are needed. We devised an innovative, sound, software-supported design approach. In particular, novel methods in data structure representation and data structure manipulation were developed by the *Microsystems and Nanotechnologies* team to ensure design specifications and objectives. We synthesize and utilize the linear word-level decision diagrams (LWDDs) that allow us to perform the compact representation of logic circuits utilizing linear arithmetical polynomials (LP) [11, 12]. The design complexity becomes $\boldsymbol{O(n)}$. The proposed design concept ensures compact representation of circuits compared with other formats and methods. The following design algorithm guarantees compact circuit representation:

Function (Circuit) ↔ BDD Model ↔ LWDD Model ↔ Realization.

The LWDD is embedded in 3D $\aleph$-hypercells that represent circuits in a 3D space. The polynomial representation of logical functions ensure the description of multi-output functions in a word-level format. The expression of a Boolean function f of n variables (x_1, x_2, … x_{n-1}, x_n) is $LP = a_0 + a_1x_1 + a_2x_2 + ... + a_{n-1}x_{n-1} + a_nx_n = a_0 + \sum_{j=1}^{n} a_j x_j$. To perform a design in 3D, we established the following mapping LWDD(a_0,a_1,a_2,…,a_{n-1},a_n) ↔ LP. The nodes of LP correspond to a Davio expansion. The LWDD is used to represent any m-level circuit with levels L_i, i=1, …, m with elements of the standard primitive library. Two data structures defined in the algebraic form by a set of LPs as

$$L = \begin{cases} L_1 : \text{inputs } x_j ; \text{outputs } y_{1k} \\ L_2 : \text{inputs } y_{1k} ; \text{outputs } y_{2l} \\ ..... \\ L_{m-1} : \text{inputs } y_{m-2,t} ; \text{outputs } y_{m-1,w} \\ L_m : \text{inputs } y_{m-1,w} ; \text{outputs } y_{m,n} \end{cases}$$

that corresponds to $LP_1 = a_0^1 + \sum_{j=1}^{n_1} a_j^1 x_j, ..., LP_m = a_0^n + \sum_{j=1}^{n_m} a_j^n y_{m-1,j}$,

or in the graphic form by a set of LWDDs as $LWDD_1(a_0^1,...,a_{n_1}^1) \leftrightarrow LP_1, ..., LWDD_m(a_0^n,...,a_{n_m}^n) \leftrightarrow LP_m$.

The use of LWDD is a significant departure from existing logic design tools but our technology is compatible with the existing software, algorithms and circuit representation formats. Circuit transformation, format transformation, modular architecture, library functions over primitives, and other features can be performed. From the circuit transformation viewpoint, all combinational circuits can be represented by LWDD. The format transformation can be performed for circuits defined in Electronic

Data Interchange Format - EDIF, Berkeley Logic Interchange Format - BLIF, Verilog and other formats. The library functions may have a library of LWDDs for multi-input circuits, as well as libraries of molecular electronic devices and ^{M}gates. The important feature is that these primitives are realized (through logic design), and should be fabricated as $\aleph$-hypercells modules. The reported LWDD provides modeling, analysis, verification, evaluation and other features.

Arithmetic expressions underlying the design of LWDD are canonical representations of logic functions. They are alternatives of the sum-of-product, product-of-sum and Reed–Muller forms of representation of Boolean functions. In LWDDs, linear data structures are manipulated using the masking operators. In particular, LWDDs are obtained by mapping LPs, where the nodes correspond to the Davio expansion and functionalizing vertices to the coefficients of the LPs. The LWDD design flow is

Primitive ↔ LP Model ↔ LWDD Model ↔ Realization.

Any *m*-level logic circuits with fixed order of elements are uniquely represented by a system of *m* LWDDs as: Function (Circuit) ↔ LP Model ↔ LWDD Model ↔ Realization. The proposed concept is verified by representing Boolean functions by hypercells in 3D ICs design. CAD tools for logic design must be based on the principles of 3D realization of logic functions with a library of primitives. LWDDs are extended by embedding the total solution tree into the $\aleph$-hypercell structures. For two graphs $G=(V,E)$ and $H=(W,F)$, we embed the graph G into the graph H. The information in the resulting $\aleph$-hypercells is subdivided according to the new structural properties of the cell and the type of the embedded tree. The embedding of a guest graph G into a host graph H is a one-to-one mapping M_{GV}: $V(G)\rightarrow V(H)$, along with the mapping M that maps an edge $(u;v)\in E(G)$ to a path between $M_{GV}(u)$ and $M_{GV}(v)$ in H. Thus, the embedding of G into H is a one-to-one mapping of the nodes in G to the nodes in H.

3. 1. 3. Information-Theoretic Analysis

Consider the input-output information measures for 3D ICs as shown in Figure 4. One examines the information carried by the variable x_i and function f, denoted as $I(x_i)$ and $I(f)$, as well as entropies of the input variable x_i and the output function f, denoted as $H(x_i)$ and $H(f)$. The condition entropies $H(f|x_i)$ and $H(x_i|f)$, relative information $I(f|x_i)$ and $I(x_i|f)$, mutual information $I(f,x_i)$, as well as joint entropy $H(f,x_i)$ are of our interest.

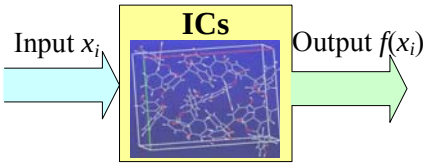

Figure 4. Input-output representation of ^{M}ICs

In design, decision diagrams and decision trees are used. Information measures can be estimated and evaluated. Decision trees are designed using the Shannon and Davio expansions and information theoretical approaches [12]. There is a need to find the best variable and expansion for any node of the decision tree in terms of information measures in order to minimize or maximize information estimates. The entropy-based optimization algorithm should generate the *optimal paths* in a decision tree with respect to the design criterion. The decision tree is designed by arbitrarily choosing any variable using Shannon (S), positive Davio (pD) or negative Davio (nD) expansions for each node. We use the conditional entropy $H(f|Tree)$ and mutual information $I(f,Tree)$ as the performance estimates. The *initial*

state of the design process is characterized by the maximum value for the conditional entropy $H(f|Tree)=H(f)$. Nodes are recursively attached to the decision tree by minimizing the entropy $H(f|Tree)$ and maximizing the mutual information $I(f,Tree)$. The final state of the decision tree is characterized by $H(f|Tree)=0$ and $I(f;Tree)=H(f)$.

The decision tree design process is a recursive decomposition of a switching function. This recursive decomposition corresponds to the expansion of switching function f with respect to the variable x. The variable x carries information that influences f. The initial state of the expansion $\sigma\in\{S,pD,nD\}$ can be characterized by the entropy $H(f)$, and the final state by the conditional entropy. In particular, the σ-expansion of the function f with respect to the variable x is $I^{\sigma}(f,x) = H(f) - H^{\sigma}(f|x)$. The information estimates for S, pD and nD expansions are found. If the design of a decision tree is based on the S expansion and the sum-of-products mapping, then, the information measure for the function f with respect to x is $H^{S}(f|x) = p_{|x=0}\cdot H(f_{|x=0}) + p_{|x=1}\cdot H(f_{|x=1})$. The information measure of the S expansion is the conditional entropy, e.g., $H^{S}(f|x)=H(f|x)$. In contrast, for the pD and nD expansions, we have $H^{pD}(f|x) = p_{|x=0}\cdot H(f_{|x=0}) + p_{|x=1}\cdot H(f_{|x=0}\oplus f_{|x=1})$ and $H^{nD}(f|x) = p_{|x=1}\cdot H(f_{|x=1}) + p_{|x=0}\cdot H(f_{|x=0}\oplus f_{|x=1})$. The information-theoretic estimates of the pD and nD nodes, as compared with the Shannon expansion, for a decision tree design are $\Delta I^{pD} = p_{|x=1}\cdot\left[H(f_{|x=1}) - H(f_{|x=0}\oplus f_{|x=1})\right]$ and $\Delta I^{nD} = p_{|x=0}\cdot\left[H(f_{|x=0}) - H(f_{|x=0}\oplus f_{|x=1})\right]$. Our results justify the use of the Davio expansions in the design as illustrated for the benchmarking circuits. It is found that the information estimates are one of the criteria to optimize 3D design as well as ICs. The following example illustrates the concept.

Example. Consider the benchmark C17 circuit implemented using 3D molecular NAND gates (^{M}NAND) as reported in Figure 5.

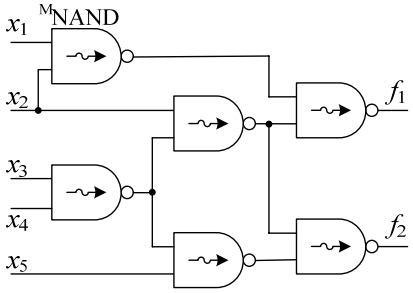

Figure 5. C17 implemented using ^{M}NAND gates

For the Shannon expansion used in the design of decision diagram, from $p(f_1=0)=14/32$ and $p(f_1=1)=18/32$, we have $H^{S}(f_1)=-(14/32)\log_2(14/32)-(18/32)\log_2(18/32)=0.99$ and $H^{S}(f_1|x_1)=-(10/32)\log_2(10/16)-(6/32)\log_2(6/16)-(4/32)\log_2(4/16)-(12/32)\log_2(12/16)=0.88$. One also obtains $H^{S}(f_1|x_2)=0.67$, $H^{S}(f_1|x_3)=0.98$, $H^{S}(f_1|x_4)=0.98$ and $H^{S}(f_1|x_5)=0.99$. The entropies $H^{S}(f_2)$ and $H^{S}(f_2|x)$ are straightforwardly calculated. The output variables and conditional entropies are found with respect to all variables if the positive and negative Davio expansions are applied. We have $H^{S}(f_1|x_i)_{\min}=0.67$, $H^{pD}(f_1|x_i)_{\min}=0.88$ and $H^{nD}(f_1|x_i)_{\min}=0.75$.

We conclude that the information-centered optimization of ICs design is formulated as the optimization algorithm with respect to the information criterion (estimates) in order to design optimal decision diagrams. A path in the decision tree starts from a node and finishes in a terminal node. Each

path corresponds to a term in the final expression for f. The criterion for choosing the decomposition variable x and the expansion $\sigma \in \{S, pD, nD\}$ is that the conditional entropy of the function with respect to this variable has to be minimum, e.g., $\min H^{\sigma}(f|x)$.

3. 1. 4. Design of Benchmarking 3D ICs and Proof-of-Concept Arithmetic Logic Unit

The proposed design of 3D ICs is illustrated and verified using benchmarking ICs. These ICs are used to evaluate and examine different design concepts. The design technology is concurrently supported by the representative CAD tools as reported in section 3.3. A series of numerical studies were conducted to accomplish the software-supported logic design for proof-of-concept ICs in 3D. The size of LWDDs generated by the developed software is compared with the best results obtained by using the Decision Diagram Packages, developed by University of Colorado and Darmstadt University of Technology, for 2D VLSI design. The method was reported and software algorithms were tested and validated. The number of nodes, number of levels and CPU time (in seconds) required to design decision diagrams for 3D ICs are reported in Table 1. The logic designs for a 9-bit ALU (c5315) and multiplier (c6288), for which classical decision diagram may not be used, were successfully performed.

Table 1. Size (number of nodes N, levels L and CPU time) in BDD, WDD and LWDD

Circuit I/O	BDD WDD	LWDD (EDIF)			LWDD (ISCAS'85)		
	#*N*	#*L*	#*N*	CPU Time	#*L*	#*N*	CPU Time
C432 36/7	1064 1209	21	455	<0.01	17	336	<0.01
C880 60/26	4053 4048	35	604	<0.01	24	605	<0.1
c2670 233/140	1850 3939	40	1374	<0.1	32	2026	<0.1
ALU c5315 178/123	1719 2504	68	3192	<0.3	49	4156	<0.4
Multiplier c6288 32/32	– –	124	4320	<0.2	124	4318	<0.5

Our goal is to evaluate 3D architecture characteristics such as volumistic size, topological parameters and performance. We assume: (1) feedforward neural networked topology with no feedback; (2) threshold ^{M}gates are used as the processing units; (3) aggregated networked 3D $\aleph$-hypercells comprised from ^{M}gates; (4) multilevel combinational circuits are used over the library of NAND, NOR and EXOR ^{M}gates. Experiments were conducted for circuits reported in Tables 1 and 2. The space size is given by X, Y and Z that result in the volumistic (V) quantity as $V=X\times Y\times Z$. The topological characteristics are evaluated using the total number of terminal (# N_T) and intermediate (# N_I) nodes. A 3D 9-bit ALU (c5315) with 178 inputs and 123 outputs is implemented using 1413 ^{M}gates, while a c6288 multiplier (32 inputs and 32 outputs) has 2327 ^{M}gates. As reported in Table 2, ^{M}gates (#G) were networked and aggregated (grouped) in 3D. The number of incompletely specified $\aleph$-hypercells was minimized. The $\aleph$-hypercells in the ith layer were connected to the corresponding hypercells in (i–1)th and (i+1)th layers. The obtained 3D architecture has $X\times Y\times Z$ hypercells. The number of terminal nodes and intermediate nodes are 3750 and 2813 for a 9-bit ALU, while, for a multiplier, we have 9248 and 6916 nodes. To combine all layers, more than 10,000 connections were generated. The design in 3D was performed within 0.4 seconds. Other metrics to evaluate the designed 3D ICs were used. That is, in addition to conventional parameters (diameter, dilation cost, expansion, load, etc.), we used the number of variables in the logic function described by $\aleph$-hypercells, number of links, fan-out of the intermediate nodes, statistics, etc.

Table 2. Experimental results for 3D ICs

Circuit I/O	Space Size				Nodes and Connections		
	#G	*#X*	*#Y*	*#Z*	$\#N_T$	$\# N_I$	CPU Time
c432 36/7	126	66	64	66	2022	1896	<0.01
c880 60/26	130	70	72	70	612	482	<0.1
c2670 233/140	828	82	80	78	3594	2766	<0.1
ALU c5315 178/123	1413	138	132	126	3750	2813	<0.4
Multiplier c6288 32/32	2327	248	248	244	9246	6916	<0.5

Comparison of 2D and 3D designs for a 9-bit ALU. The high-level model is documented in Figure 6. The studied ALU performs arithmetic and logic operations simultaneously on two 9-bit input data words, as well as computes the parity of the results. Conventional 2D logic design of a 9-bit ALU (c5315) with 178 inputs and 123 outputs results in 2406 gates. In contrast, the proposed design (as an envisioned SLSI) leads to 1413 ^{M}gates that are networked and aggregated in 3D.

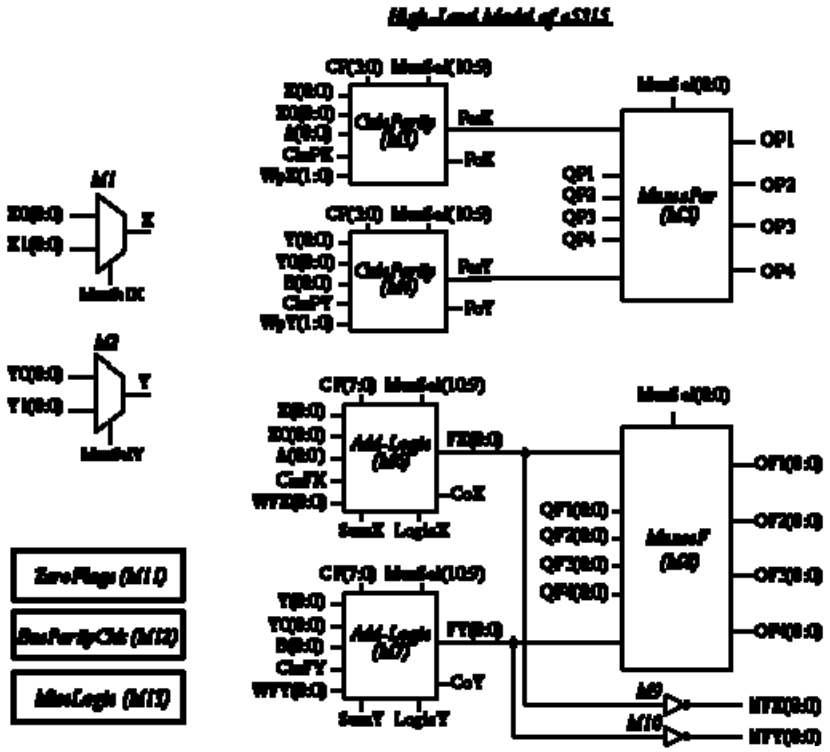

Figure 6. High-level model for a 9-bit ALU (c5315)

3. 2. ℵ-HYPERCELL DESIGN

The binary tree is a networked architecture that carries information about dual connections of each node. The binary tree also carries information about functionality of the logic circuit and topology. The nodes of the binary tree are associated with the Shannon and Davio expansions with respect to each variable and coordinate in 3D. A node in the binary decision tree realizes the Shannon decomposition $f = x_i f_0 \oplus x_i f_1$, where $f_0 = f\big|_{x_i=0}$ and $f_1 = f\big|_{x_i=1}$ for all variables in *f*. Thus, each node realizes the Shannon expansion, and the nodes are distributed over levels. The classical hypercube contains 2^n nodes, while the ℵ-hypercells has $2^n + \sum_{i=0}^{n} 2^{n-1} C_i^m$ nodes in order to design technology-dependent biomolecular ICs in 3D. The ℵ-hypercell consists of terminal nodes, intermediate nodes and roots. The most straightforward ℵ-hypercell implementation is provided by using molecular multiplexers (^{M}MUX). However, other ^{M}gates can be utilized as well. The design steps are:

Step 1: Connect the terminal node with the intermediate nodes;
Step 2: Connect the root with two intermediate nodes located symmetrically on the opposite faces;
Step 3: Pattern the terminal and intermediate nodes on the opposite faces and connect them via the root.

The nanobiocomputing architectures can be designed and implemented as aggregated ℵ-hypercells engineered (fabricated) from organic or bio molecules. Figure 7.a reports a 3D ℵ-hypercell which comprises from a two-to-one molecular multiplexer (^{M}MUX). A Molecular multiplexer and other ^{M}gates (^{M}inverter, ^{M}AND, ^{M}NAND, ^{M}OR, ^{M}NOR and ^{M}XOR), designed by the *Microsystems and Nanotechnologies* team using cyclic carbon-based molecules, are reported in Figure 7.b.

There are several methods for representing logic functions. A ℵ-hypercell, proposed as a core solution, is a homogeneous aggregated assembly for massive super-high-performance parallel computing. We apply the enhanced switching theory integrated with a novel logic design concept [12]. In the design, the graph-based data structures and 3D circuit topology are utilized. The ℵ-hypercell is a topological representation of a switching function by a *n*-dimensional graph. In particular, the switching function *f* is given as

$$\underset{f}{\text{Switching Function}} \Rightarrow \underset{\text{Operation}}{\overset{2^n-1}{\underset{i=0}{\mathbf{L}}}} \overset{\text{Coefficient}}{\mathbf{K}_i} \left(x_1^{i_1} \ldots x_n^{i_n}\right) \Rightarrow \underset{f_F}{\text{Form of Switching Function}} .$$

The data structure is described in matrix form using the truth vector ***F*** of a given switching function *f* as well as the vector of coefficients **K**. The logic operations are represented by **L**. ℵ-hypercells compute *f*, and complex switching functions are implemented by hypercells. For example, Figure 8 reports a ℵ-hypercell to implement $f = \bar{x}_1 x_2 \vee x_1 \bar{x}_2 \vee x_1 x_2 x_3$. From the technology-specific viewpoints, we propose a ℵ-hypercell solution that employs ^{M}gates as documented in Figures 7 and 8. This 3D solution coherently maps the device- and gate-level consideration by aggregating and networking ^{M}gates. By utilizing the root and intermediate nodes at the edges, as shown in Figure 8, the reported ℵ-hypercells implement switching functions *f* of arbitrary complexity.

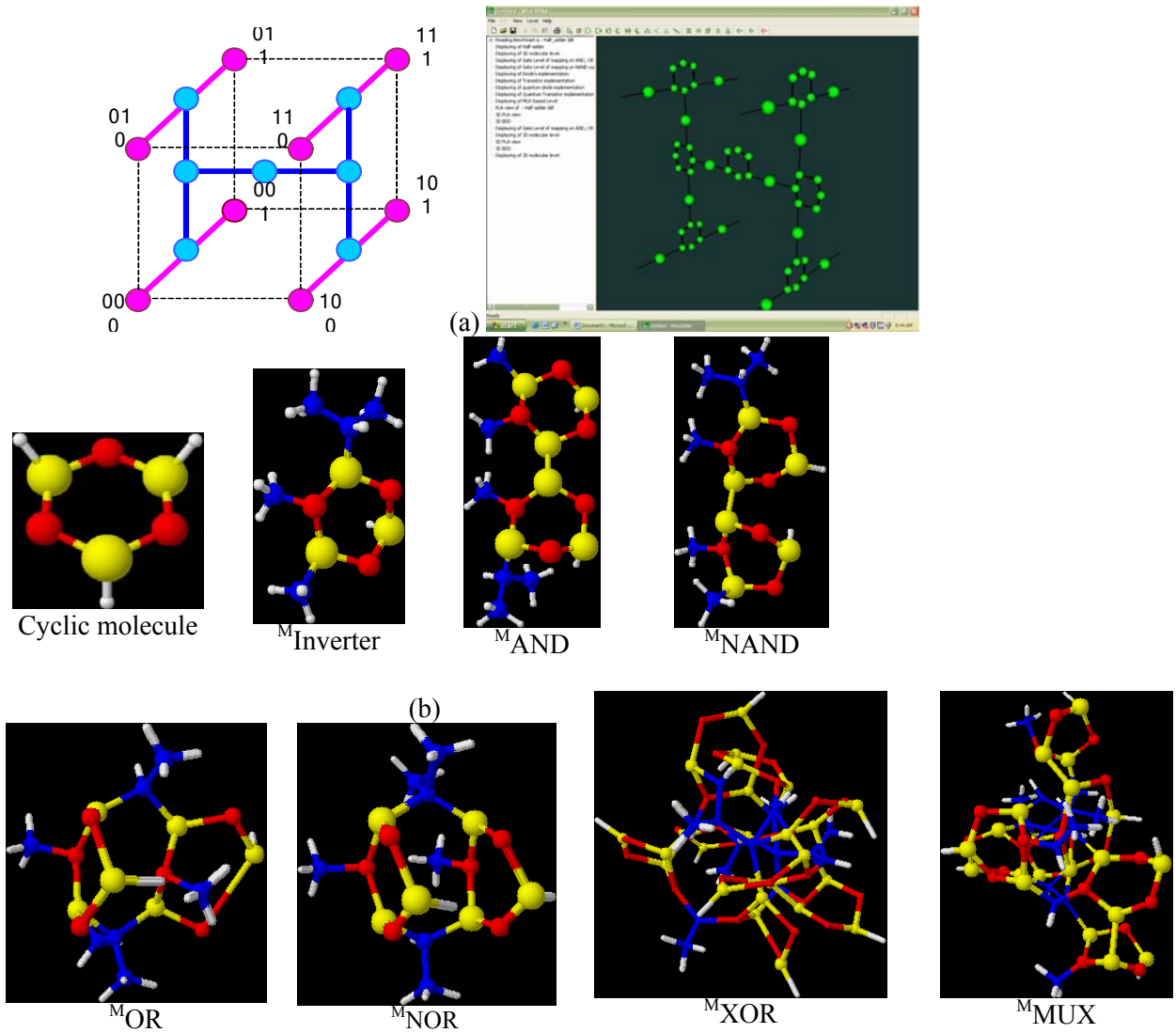

Figure 7. a) ℵ-hypercell utilizing two-to-one multiplexer (^{M}MUX);
b) ^{M}gates (^{M}inverter, ^{M}AND, ^{M}NAND, ^{M}OR, ^{M}NOR, ^{M}XOR and ^{M}MUX) which can be utilized in the design of ℵ-hypercells

The logic design in spatial dimensions was based on the advanced methods and enhanced data structures to satisfy a 3D topology. The appropriate data structure of logic functions and methods of embedding this structure into ℵ-hypercells were found. The three-step-solution in a logic functions' manipulation in order to change the carrier of information from the algebraic form (logic equation) to the hypercell structure is:

Step 1: Logic function is transformed to the appropriate algebraic form (Reed-Muller, arithmetic or word-level in matrix or algebraic representation);

Step 2: Derived algebraic form is converted to the graphical form (decision tree, decision diagram or logic network);

Step 3: Obtained graphical form is embedded, and technologically implemented, by ℵ-hypercells.

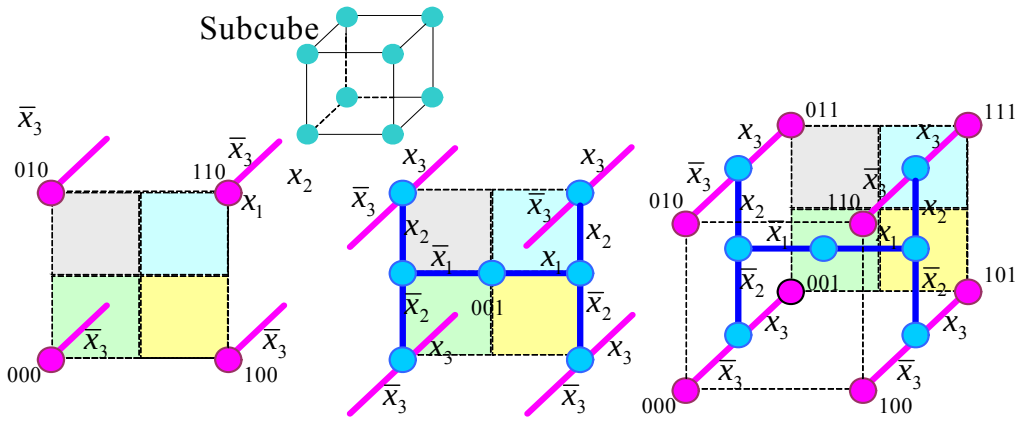

Figure 8. ℵ-hypercell that implement function *f*

The design is expressed as

$$\underset{\text{Step 1}}{\text{Logic Function}} \Leftrightarrow \underset{\text{Step 2}}{\text{Graph}} \Leftrightarrow \underset{\text{Step 3}}{N\text{ - Hypercell Structure}} .$$

The proposed procedure results in:

- Algebraic representation and robust rules of manipulation for complex switching logic functions;
- Matrix representation and sound manipulation;
- Consistency of logic relationships for variables and functions from the spectral theory viewpoint due to the use of matrix algebra;
- Graph-based representation is found using decision trees, decision diagrams and logical networks;
- Data structures are embedded into ℵ-hypercells.

3. 3. THREE-DIMENSIONAL NANOBIOCOMPUTING CAD

Fully featured technology-dependent CAD for SLSI design is a significant task that is not within the scope of this contract. The representative CAD tools and software solutions were developed in order to demonstrate the 3D design feasibility. In particular, we developed a Linear Decision Diagram (LDD) Package and Windows-Based 3D ICs Interactive Toolbox (WindowIT) using C and OpenGL. We plan to integrate both packages. The compatibility with hardware description languages is important. To be compatible with conventional logical programming tools, three netlist formats (Electronic Data Interchange Format - EDIF, International Symposium on Circuits and Systems - ISCAS, and Berkeley Logic Interchange - BLIF) are used and embedded in the LDD Package. The methods reported in sections 3.1 and 3.2 were used in the software development. A coherent data-intensive analysis of SLSI-designed ICs can be performed by a completely-featured CAD as molecular bioelectronics technology is developed. We can examine baseline characteristics and prove the efficiency, robustness, feasibility and other significant advantages of the proposed technology.

The representative components of the developed CAD prototype (LDD Package and WindowIT), allow one to carry-out the design of ICs in 3D, as well as to examine major performance estimates. The software, developed by *Microsystems and Nanotechnologies*, was successfully tested and verified. The LDD Package, based on our synthesis concept as reported in sections 3.1 and 3.2, features:

- new sound design technology and methods for 3D ICs;
- synthesis and partitioning linear decision diagrams for given functions or circuits;
- spectral representation of logic functions;
- circuit verification;
- compact format for rapid-prototyping;
- compressed representation of complex logic networks.

Results in design and visualization of 3D ICs are reported in Figure 9 displaying the Command Windows data for the LDD Package. It should be emphasized that the results of the 3D design of a c17 circuit as well as a 9-bit ALU (c5315) are displayed. The WindowIT environment is documented in Figure 10. As were reported in sections 3.1 and 3.2, we were able to successfully carry-out and verify 3D design for benchmarking ICs.

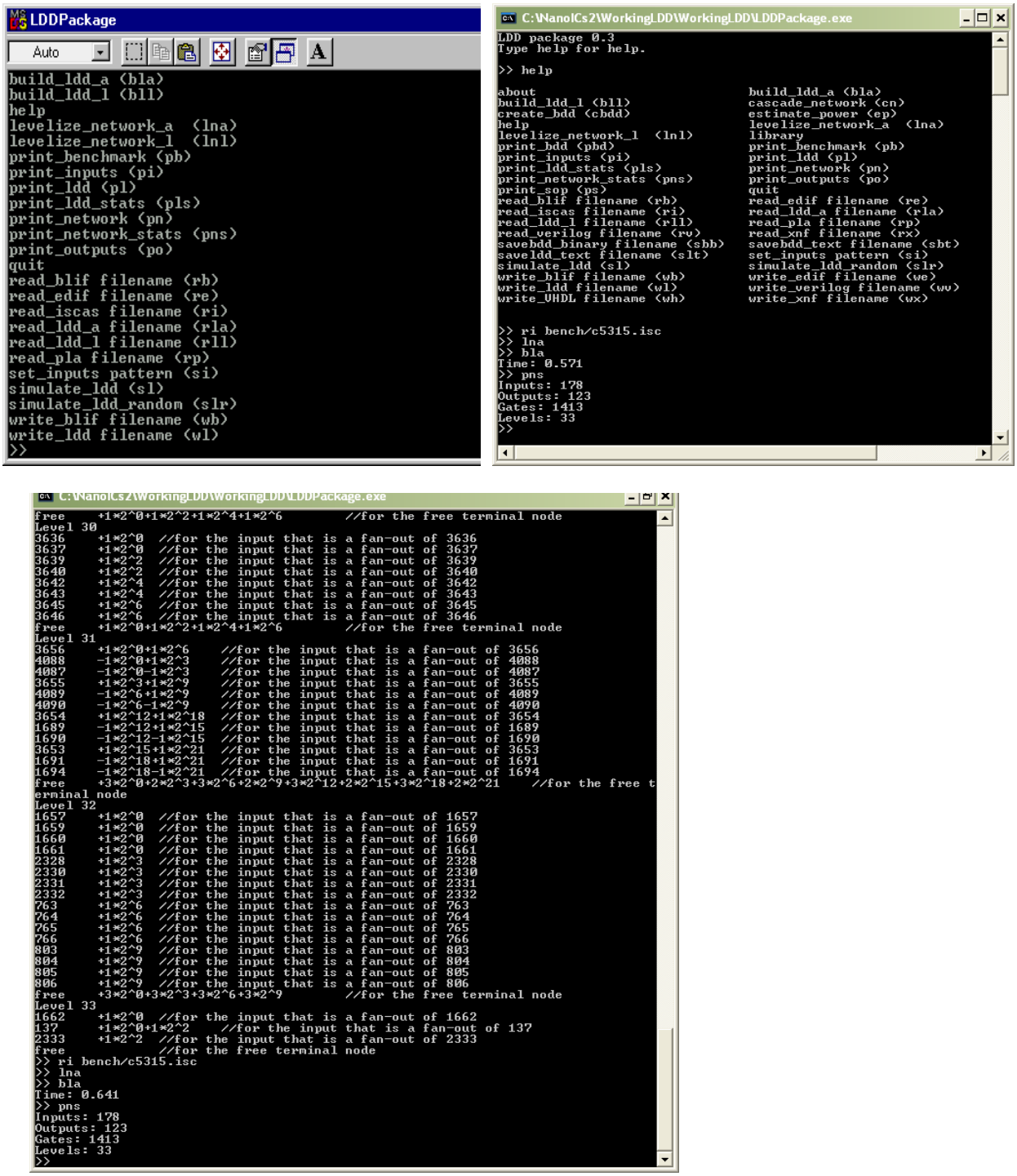

Figure 9. Design of 3D ICs using LDD Package that performs integrated design, aggregation, analysis, optimization and evaluation

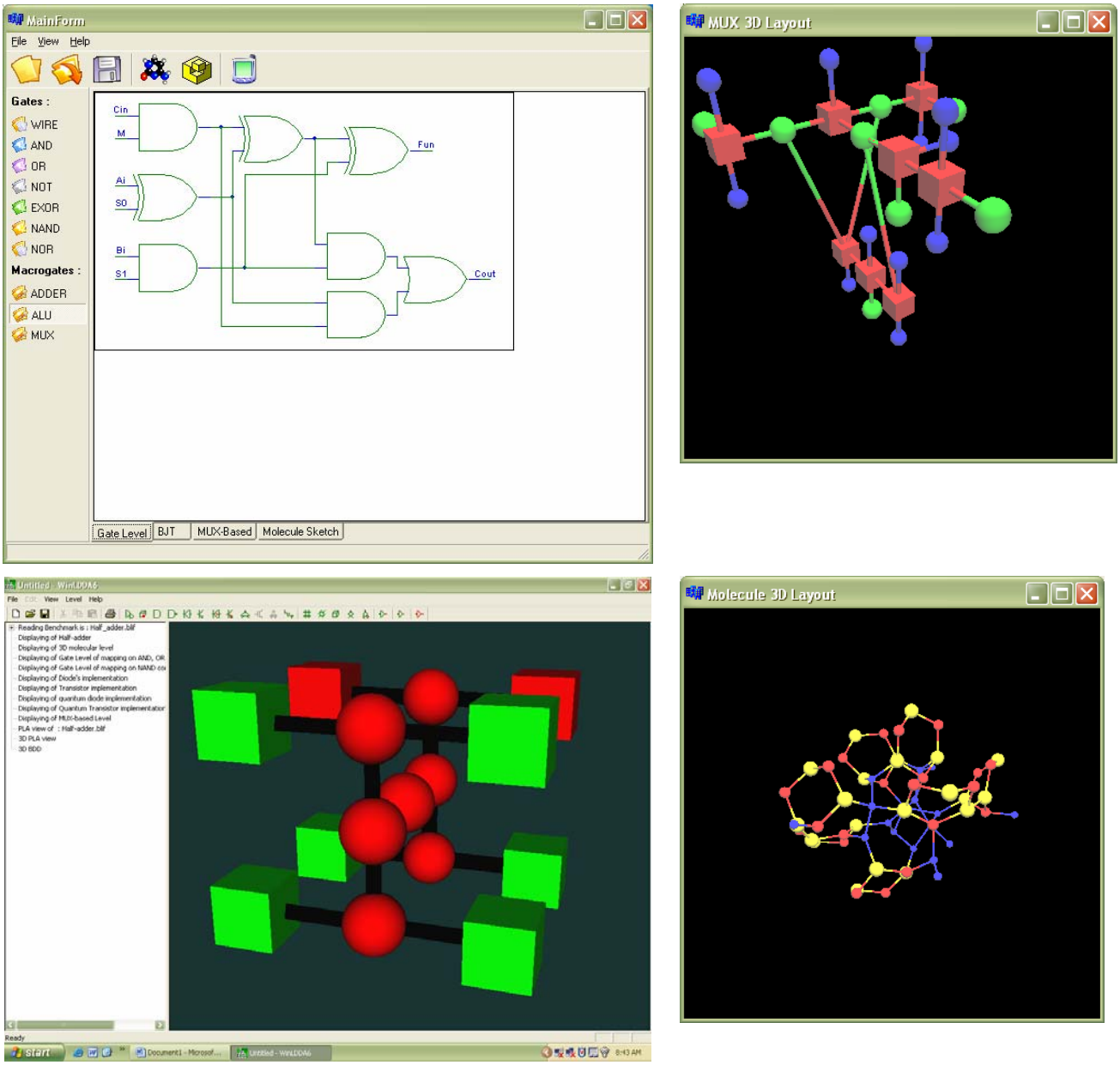

Figure 10. Design of 3D ICs using interactive WindowIT that performs integration, aggregation and visualization

3. 4. DNA DERIVATIVE TRANSISTOR FOR ℵ-HYPERCELLS

Sequence-dependent self-assembled DNA and templated protein synthesis can be used to build patterned two- and three-dimensional structures with the desired geometrical topologies [13, 14]. Some inorganic, organic, hybrid and biomolecules which exhibit desired electronic properties can be utilized in a new generation of electronic nanodevices and in nano-bio-electronic architectures [2, 4, 15-17]. Complex 3D information processing, computing and memory architectures are envisioned to be designed and fabricated using self-assembled biomolecules (including DNA and proteins) utilized as enhanced-functionality multi-terminal interconnected electronic nanobiodevices. It is important to design and analyze functional high-performance bioelectronic devices while taking basic phenomena and effects in biomolecule–interconnect complexes into account. Insulating, conducting and semiconducting properties have been observed in the contact–biomolecule–contact and inter-biomolecular complexes [18-20]. DNA synthesis, sequence, length, environment, alignment and other factors influence the electronic characteristics. In DNA, various experiments to examine the charge and electron transport, *I–V* characteristics, conductance and other electronic properties were performed in [18-20] with limited success. Figure 11.a illustrates DNA attached to two electrodes [19]. The electrode (source and drain) electrochemical potentials are denoted as V_{Fs} and V_{Fd}, while E_s and E_d are the self-energy functions of the source and drain. Electrochemical potentials V_{Fs} and V_{Fd} vary. There is no electron transport if the system is in equilibrium, e.g., $V_{Fs} = V_{Fd}$. The highest occupied molecular orbitals (HOMO) and lowest unoccupied molecular orbitals, (LUMO), as well as the Fermi level, are illustrated. Depending on the HOMO and LUMO levels, as well as E_F, the electron transport takes place through the particular orbitals. Using broadening energies E_{Bs} and E_{Bd}, the electron transfer rates are E_{Bs}/h and E_{Bd}/h. Guanine quartets (tubular sequences of G tetramers) were reported [19]. Tetramers (G4) are the building blocks of a quadruple-helix forming G4-DNA. The hydrogen-bonded guanines arrange in a 2.3 nm diameter configuration. The G4-DNA-based multi-terminal electronic nanodevice is illustrated in Figure 11.b. Though G4-DNA aggregates were fabricated, the electronic characteristics have not been experimentally examined due to unsolved interconnect, manipulation and characterization difficulties.

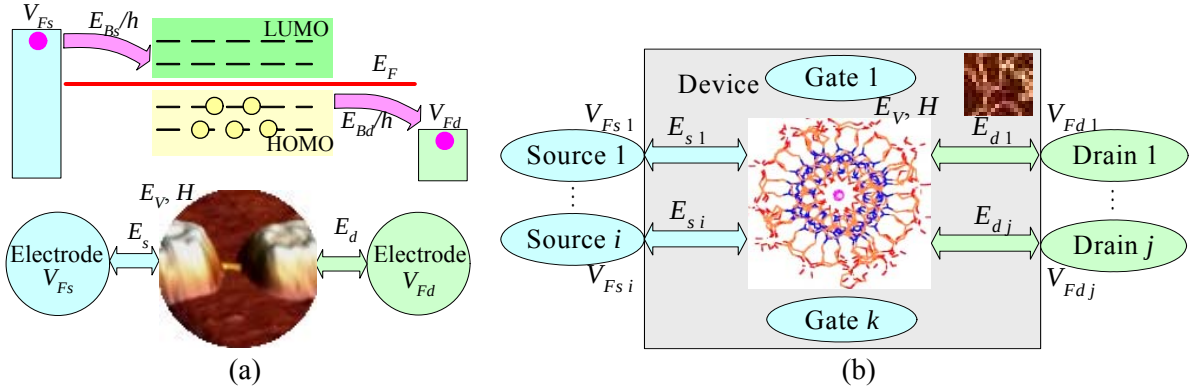

Figure 11. a) Double-stranded DNA with two electrodes;
b) G4-DNA-based multi-terminal electronic nanodevice and 3D nanobioICs topology

Due to the limited experimental data for the electron transport and *I–V* characteristics in biomolecules, we examined a hybrid CMOS-technology device for which the experimental data is available [21, 22]. Prototypes of hybrid bioelectronic devices were built by utilizing enhanced CMOS technology. The electronic behavior and *I–V* characteristics in the planar topology DNA-based transistor (DNA^T), as reported in Figure 12.a, were studied merging experimental and theoretical results. The

studied DNA^T is equivalent, to some extent, to the silicon technology CMOS field-effect transistors (FET). For the planar DNA^T, the experimental *I–V* characteristics were measured as documented in Figure 12.b.

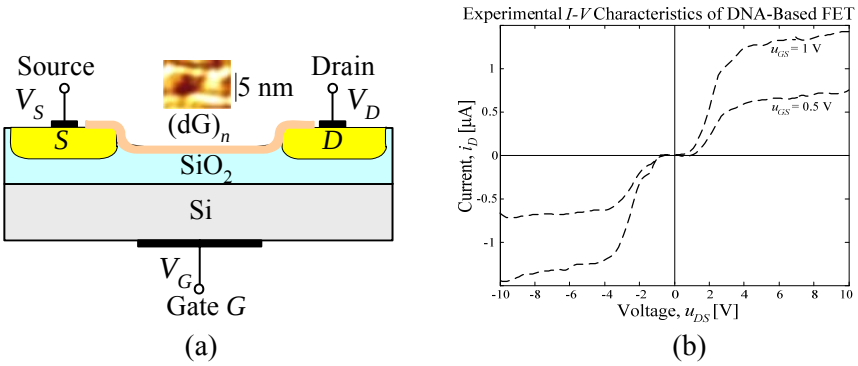

Figure 12. DNA^T and experimental *I–V* characteristics

The fabrication of this DNA^T is performed utilizing CMOS technology and depositing A-DNA on silicon oxide with the adsorption-based source–DNA–drain interconnect. It is reported that an A-DNA bundle of poly(dA)-poly(dT) is a *n*-type semiconductor, while poly(dG)-poly(dC) is a *p*-type [22]. DNA derivatives may ensure self-assembled and ordered engineered bundles, layers and ropes which are organized and interconnected due to specific reactivity of molecules' functional groups with affinity to distinct surfaces and molecules. The guanine (DNA nitrogenous base) exhibits a low oxidation potential that results in electron transport and self-assembly in liquid and solid media [23]. DNA^T with self-organized H-bonded DNA bases were studied in [21-23] utilizing a polymerized derivative of deoxyguanosine poly(dG)$_n$. A single modified DNA base, e.g., poly(dG)$_n$, is deposited on the silicon oxide between source and drain as reported in Figure 12.a forming the channels. The experimental *I–V* characteristics are documented for a different voltage $u_{GS,}$, which controls the electron flow in the source–drain channel.

The modeling is performed using the Green's function formalism [4, 24-27]. The Hamiltonian (H) for the open contact (left and right electron reservoirs) – biomolecule (bridge) complex is constructed by using the biomolecule H_M, tunneling H_T, contact (junction) H_C and external H_E Hamiltonians. That is, we have $H = H_M + H_T + H_C + H_E$. To derive the *I–V* characteristics of the biomolecular complex (electrode–biomolecule–electrode), we apply Keldysh's nonequilibrium Green function concept. Green's function is a wave function of energies at $\mathbf{r}$ resulting from an excitation applied at $\mathbf{r}_E$. We applied the retarded Green's function G that represents the response of the biomolecule–contact complex. Hence, $(E-H)G(\mathbf{r},\mathbf{r}_E)=\delta(\mathbf{r}-\mathbf{r}_E)$. The boundary conditions must be satisfied for the transport and Poisson equations. The molecular Hamiltonian of the isolated system and the complex self-energy functions are used to examine the finite biomolecule complex, instead of the single energy potential and broadening energies. In the matrix notations, using the overlap identity matrix S, the Green's function is found to be $[G(E)]=\left(E[S]-[H]-[V_{SC}]-\sum_i[E_i]\right)^{-1}$, where $[E_i]=[S_i][G_i][S_i^*]$; S_i is the geometry-dependent coupling (contact) matrix between the surface of the source/drain and biomolecule (for source and drain S_s and S_d are the geometry-dependent coupling matrices between the surface of the source and drain and the device). The imaginary non-Hermitian self-energy functions of the source and drain (first and second electron reservoirs) E_s and E_d are $[E_s]=[S_s][G_s][S_s^*]$ and $[E_d]=[S_d][G_d][S_d^*]$, where G_s and G_d are the surface Green's functions for the source and drain that are found applying the recursive methods.

Taking note of the Green's function, the density of state $D(E)$ is found using $G(E)$ as $D(E) = -\frac{1}{\pi}\mathrm{Im}\{G(E)\}$. The spectral function $A(E)$ is the anti-Hermitian term of the Green's function, and $A(E) = i[G(E) - G^*(E)] = -2\,\mathrm{Im}[G(E)]$. One obtains $D(E) = \frac{1}{2\pi}\mathrm{tr}[A(E)S]$, where tr is the trace operator, and S is the identity overlap matrix for orthogonal basis functions. Using the broadening energy functions E_{Bs} and E_{Bd}, one obtains the source and drain spectral functions $[A_s(E)] = [G(E)][E_{Bs}(E)][G^*(E)]$, $[A_d(E)] = [G(E)][E_{Bd}(E)][G^*(E)]$.

For multi-terminal electronic nanobiodevices, the nonequilibrium charge density matrix is

$$[\rho(E)] = \frac{1}{2\pi}\int_{-\infty}^{\infty}\sum_{k,i\in s,\,j\in d} f(E_{Vk}, V_{Fi.j})[A_{i,j}(E)]dE = \frac{1}{2\pi}\int_{-\infty}^{\infty}\sum_{k,i\in s,\,j\in d} f(E_{Vk}, V_{Fi.j})[G(E)][E_{Bi,j}(E)][G^*(E)]dE,$$

where $V_{Fi,j}$ are the potentials, e.g., V_{Fs} and V_{Fd} are the source and drain potentials related to the Fermi levels; $f(E_V,V_{Fi,j})$ are the Fermi-Dirac functions, for example, $f(E_V,V_{Fs})$ and $f(E_V,V_{Fd})$; E_V is the single energy potential that depends on the charge density $\rho(E)$, $E_V = E_{v0} + \rho(E)$. Utilizing the transmission matrix $T(E) = \mathrm{tr}[E_{Bs}G(E)E_{Bd}G^*(E)]$ and taking note of the Green's function and broadening, the current is found to be $I_k = \frac{2e}{h}\int_{-\infty}^{+\infty}\mathrm{tr}[E_{Bs}G(E)E_{Bd}G^*(E)]\sum_{k,i\in s,\,j\in d} f(E_{Vk}, V_{Fi,j})dE$.

The contact–biomolecule–contact complex attains equilibrium with the Fermi level. The current–voltage characteristics are calculated. The solutions and *I–V* characteristics are found carrying out robust heterogeneous MATLAB simulations with data-intensive analysis features. The non-equilibrium charge density is $\rho(E) = \frac{1}{2\pi}\int_{-\infty}^{\infty}\left[f(E_V,V_{Fs})G(E)E_{Bs}G^*(E) + f(E_V,V_{Fd})G(E)E_{Bd}G^*(E)\right]dE$, where $f(E_V,V_{Fs})$ and $f(E_V,V_{Fd})$ are the Fermi-Dirac functions, $f(E_V,V_{Fs}) = \left(1 + e^{\frac{E_V - V_{Fs}}{kT}}\right)^{-1}$, $f(E_V,V_{Fd}) = \left(1 + e^{\frac{E_V - V_{Fd}}{kT}}\right)^{-1}$. Hence, the current between two junctions (contacts) is $I = \frac{2e}{h}\int_{-\infty}^{+\infty}\mathrm{tr}[E_{Bs}G(E)E_{Bd}G^*(E)]\left[f(E_V,V_{Fs}) - f(E_V,V_{Fd})\right]dE$.

For the numerical studies, the LUMO and HOMO energy gaps, broadening energies, Fermi energy E_F, as well as other data are used. It should be emphasized that the polymerized derivative of deoxyguanosine poly(dG)$_n$ forms non-uniform and non-perfect channels of different length with distinct binding to the source and drain. Furthermore, the electrostatic field that affects the electron transport is non-uniform. Correspondingly, in general, one may not be able to achieve a precise matching of the experimental and analytical (numerical) results. The energy levels of the molecular orbitals, examined for the free biomolecule, thiol–biomolecule, as well as the Au–S–biomolecule–S–Au complex, are different. In analysis of electronic characteristics, one considers the biomolecule orbitals; 3s sulfur orbitals, as well as 5d, 6s and 6p gold orbitals. The HOMO and LUMO of the Au cluster shift towards lower energies upon interaction with the functionalized biomolecule. The contribution of different orbitals to the electron transport varies. Two occupied orbitals result in a strong coupling (hybridization) between gold, sulfur and the π-conjugated molecule. These orbitals are of great importance for electron transport between contacts and the functionalized molecule. The HOMO-LUMO gap is 1.75 eV. However, other

LUMOs and HOMOs contribute to the electron transport. Simulation results are reported in Figures 13 to 15 (dashed lines) for different coupling and Fermi energies of the gold cluster, assuming a single biomolecule energy level E_V. One should integrate multiple HOMO and LUMO states. Therefore, in addition to single-state modeling (numerical results are reported in Figures 13 to 15 by dashed lines), modeling and simulation with multi-level discrete energy levels were performed. The results are shown in Figures 13 to 15 as a solid line. The value of E_{V0} is $E_{V0} = (E_{LUMO} - 1.5)$ eV. Figure 16 reports the *I–V* and *G–V* characteristics if E_{V0} is close to LUMO, and, in particular, $E_{V0} = (E_{LUMO} - 0.2)$ eV. The results qualitatively explain and quantitatively match the experimental measurements of the *I–V* characteristics with distinct coupling energies, Fermi level and initial single energy potential E_{V0}. The results reported provide evidence that high-fidelity modeling and data-intensive analysis can be performed using the non-equilibrium Green function method. Furthermore, the *I–V* characteristics can be controlled (shaped) and varied utilizing organic synthesis and design.

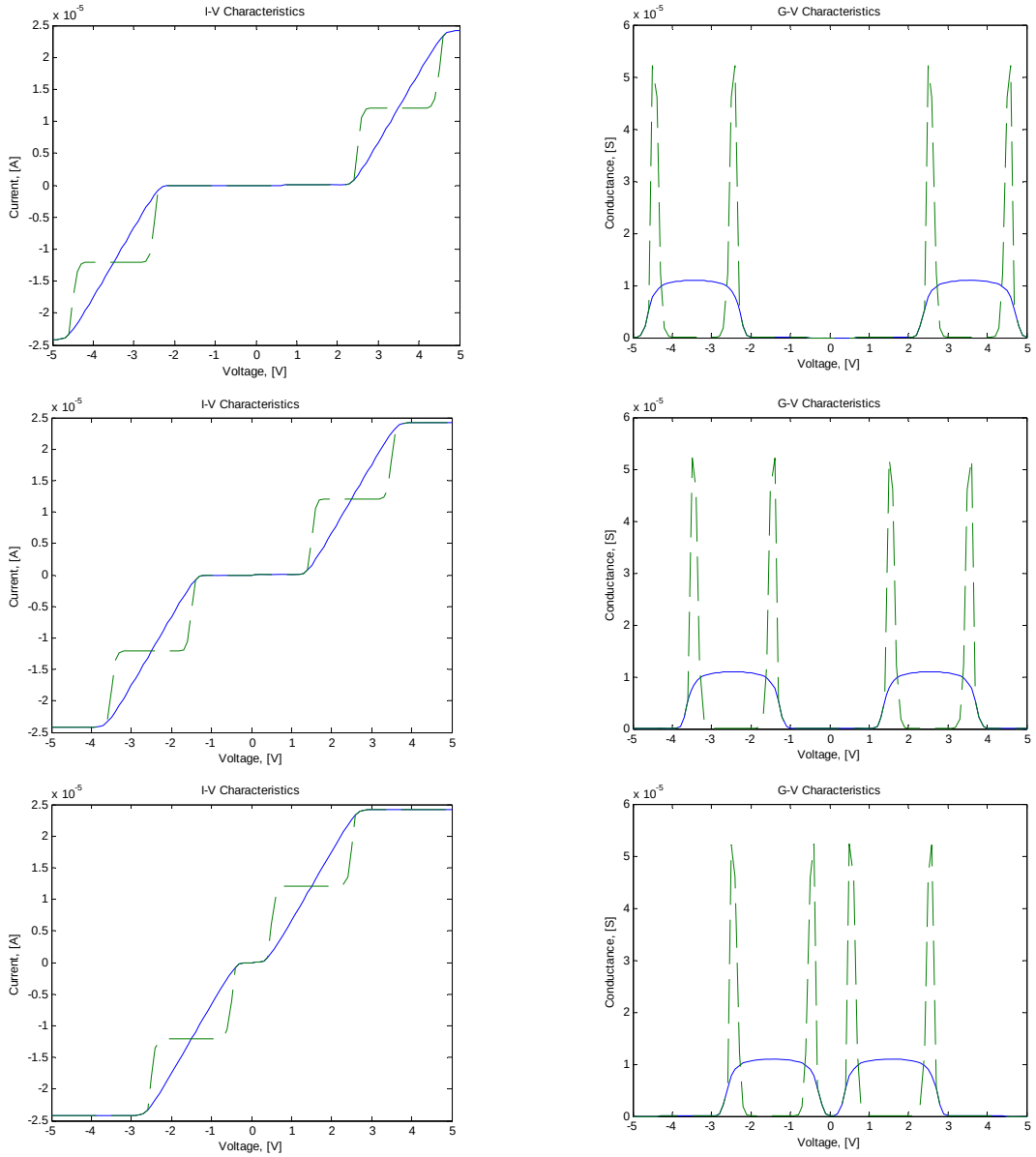

Figure 13. The *I–V* and *G–V* characteristics of DNA^T with $E_{BL} = E_{BR} = 0.1$ eV
a) $E_F = (E_{LUMO} - 0.4)$ eV; b) $E_F = (E_{LUMO} - 0.8)$ eV; c) $E_F = (E_{LUMO} - 1.2)$ eV

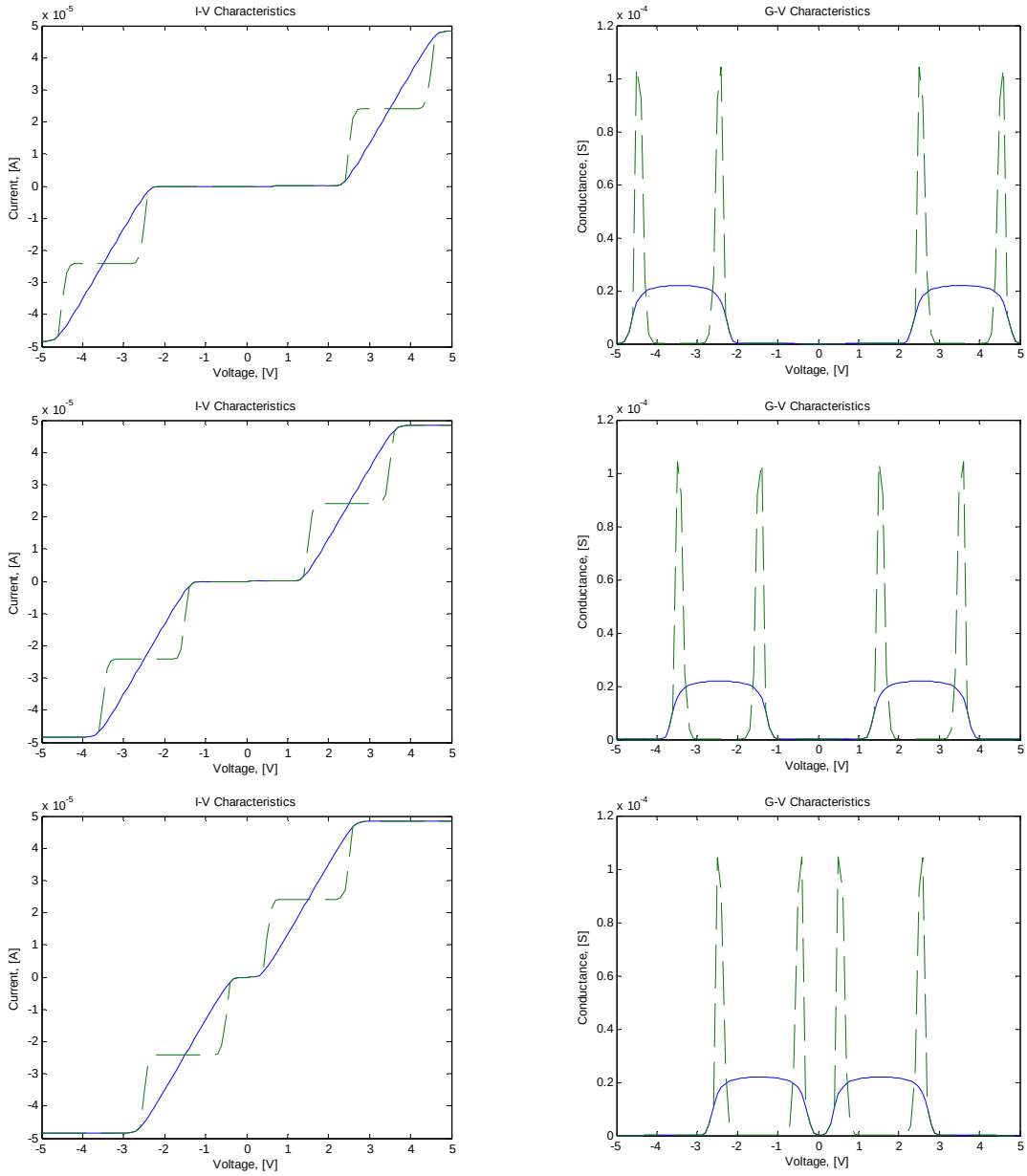

Figure 14. The *I–V* and *G–V* characteristics of DNA^{T} with $E_{BL} = E_{BR} = 0.2$ eV
a) $E_F = (E_{LUMO} - 0.4)$ eV; b) $E_F = (E_{LUMO} - 0.8)$ eV; c) $E_F = (E_{LUMO} - 1.2)$ eV

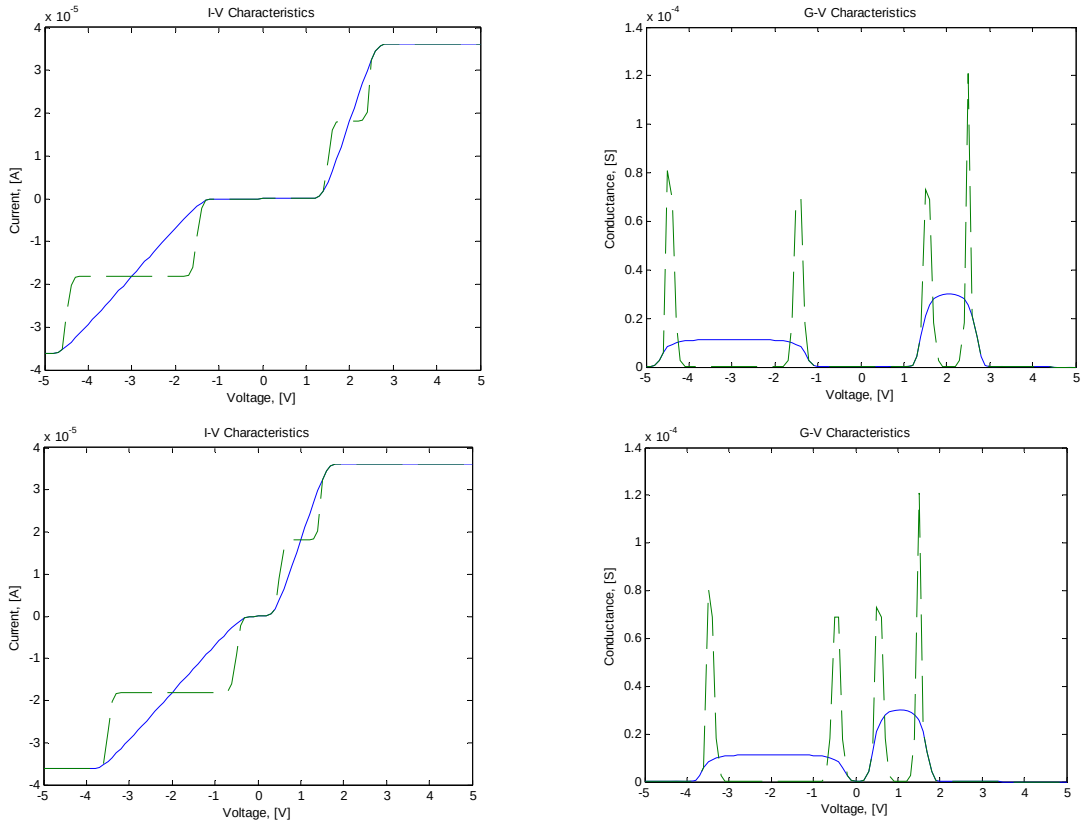

Figure 15. The *I–V* and *G–V* characteristics of DNA^T with $E_{BL} = 0.1$ eV, $E_{BR} = 0.3$ eV
a) $E_F = (E_{LUMO} - 0.8)$ eV; b) $E_F = (E_{LUMO} - 1.2)$ eV

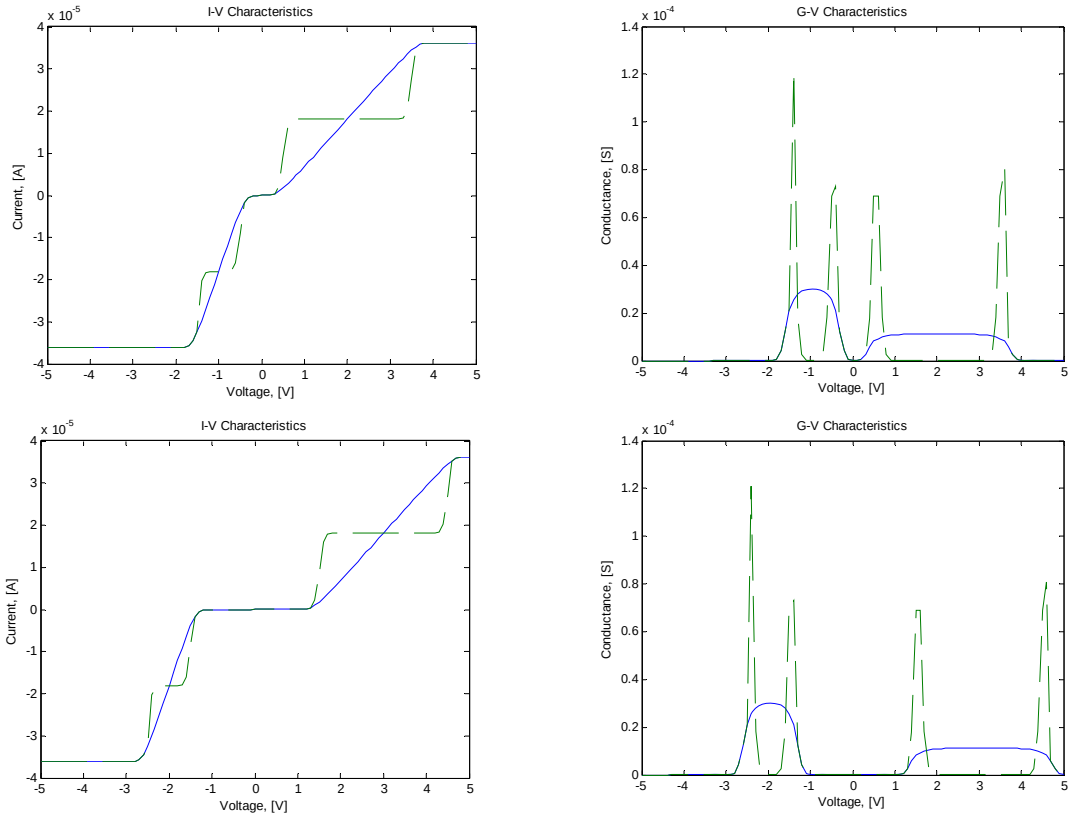

Figure 16. The *I–V* and *G–V* characteristics of DNA^T with E_{BL}= 0.1 eV, E_{BR}= 0.3 eV, E_{V0}= (E_{LUMO}–0.2) eV
a) E_F = (E_{LUMO} – 0.4) eV; b) E_F = (E_{LUMO} – 0.8) eV

The experimental and numerical results reported show a significant variation of electron transport in the DNA^T depending on potential barriers, charge distribution, quantization of energy levels, quantum interference, binding to the electrodes and other effects. The obtained *I–V* characteristics through modeling and simulation match the experimental data. The numerical and experimental data demonstrates the validity of the results. Therefore, we achieved accuracy and coherence in the ability to analyze biomolecular electronic devices.

4. Conclusions

As documented in this report, *Microsystems and Nanotechnologies* has successfully completed all Tasks outlined in the Statement of Work. A novel design concept for 3D ICs and computing architectures was developed, verified and demonstrated. The proposed design is supported by novel software and envisioned hardware technologies. For complex ICs, we performed the design by utilizing ℵ-hypercells. At the system level, benchmarking ICs (that have been widely used to evaluate 2D VLSI/ULSI design) were examined as proof-of-concept 3D ICs for the envisioned biomolecular computing architectures. At the device level, we examined a DNA^T, as a possible proof-of-concept three-terminal hybrid bioelectronic device. The aggregated ℵ-hypercells form neuronal 3D ℵ-hypertopologies, thereby implementing ICs and nanobiocomputing architectures. The representative CAD components were developed in order to coherently support the reported SLSI design for 3D ICs. *Microsystems and Nanotechnologies* has proposed a revolutionary $3D^{3\ (\text{Hardware–Software–Nanotechnology})}$ technology that ensures super-high-performance computing and information processing. We focused on development of a feasible, practical, affordable and superior technology for massive parallel distributed computing and information processing for Air Force systems.

References

1. *International Technology Roadmap for Semiconductors*, 2005 Edition, Semiconductor Industry Association (SIA), SEMATECH, Austin, Texas, USA, 2005.
2. J. C. Ellenbogen and J. C. Love, "Architectures for molecular electronic computers: Logic structures and an adder designed from molecular electronic diodes," *Proc. IEEE*, vol. 88, no. 3, pp. 386-426, 2000.
3. J. R. Heath and M. A. Ratner, "Molecular electronics," *Physics Today*, no. 1, pp. 43-49, 2003.
4. S. E. Lyshevski, *NEMS and MEMS: Fundamentals of Nano- and Microengineering*, CRC Press, Boca Raton, FL, 2005 (second edition).
5. S. E. Lyshevski, *Nanocomputers and Nanoarchitectronics*, *Handbook of Nanoscience, Engineering and Technology*, Ed. W. Goddard, D. Brenner, S. Lyshevski and G. Iafrate, pp. 6.1-6.39, CRC Press, Boca Raton, FL, 2002.
6. W. Porod, *Nanoelectronic Circuit Architectures*, *Handbook of Nanoscience, Engineering and Technology*, Eds. W. A. Goddard, D. W. Brenner, S. E. Lyshevski and G. J. Iafrate, pp. 5.1– 5.12, 2003.
7. S. R. Williams and P. J. Kuekes, "Molecular nanoelectronics," *Proc. Int. Symposium on Circuits and Systems*, Geneva, Switzerland, vol. 1, pp. 5 – 7, 2000.
8. S. Akers, "Binary decision diagrams," *IEEE Trans. Comput.*, vol. 27, no. 6, pp. 509-516, 1978.
9. R. E. Bryant, "Graph-based algorithms for Boolean function manipulation," *IEEE Trans. Comput.*, vol. 35, no. 6, pp. 677-691, 1986.
10. S. Minato, *Binary Decision Diagrams and Applications for VLSI CAD*, Kluwer, New York, 1996.
11. V. D. Malyugin, "Realization of corteges of Boolean functions by linear arithmetical polynomials," *Automica and Telemekhica*, no. 2, pp. 114-121, 1984.
12. S. Yanushkevich, V. Shmerko and S. E. Lyshevski, *Logic Design of NanoICs*, CRC Press, Boca Raton, FL, 2005.
13. A. Carbone and N. C. Seeman, "Circuits and programmable self-assembling DNA structures," *Proc. Nat. Acad. Science,* vol. 99, no. 20, pp. 12577-12582, 2002.
14. N. C. Seeman, "DNA engineering and its application to nanotechnology," *Nanotechnology,* vol. 17, pp. 437-443, 1999.
15. J. M. Tour and D. K. James, *Molecular Electronic Computing Architectures*, *Handbook of Nanoscience, Engineering and Technology*, Eds. W. A. Goddard, D. W. Brenner, S. E. Lyshevski and G. J. Iafrate, pp. 4.1–4.28, 2003.
16. J. Reichert, R. Ochs, D. Beckmann, H. B. Weber, M. Mayor and H. V. Lohneysen, "Driving current through single organic molecules," *Physical Review Letters*, vol. 88, no. 17, 2002.
17. W. Wang, T. Lee, I. Kretzschmar and M. A. Reed, "Inelastic electron tunneling spectroscopy of an alkanedithiol self-assembled monolayer," *Nano Letters*, vol. 4, no. 4, pp. 643-646, 2004.
18. D. Porath, "Direct measurement of electrical transport through DNA molecules," *Nature*, vol. 403, pp. 635-638, 2000.
19. D. Porath, G. Cuniberti and R. Di Felice, "Charge transport in DNA-based devices," *Top. Curr. Chem.*, vol. 237, pp. 183-227, 2004.
20. A. Rakitin, P. Aich, C. Papadopoulos, Y. Kobzar, A. S. Vedeneev, J. S. Lee and J. M. Xu, "Metallic conduction through engineered DNA: DNA nanoelectronic building blocks," *Physical Review Letters*, vol. 86, no. 16, pp. 3670-3673, 2001.
21. R. Rinaldi, E. Branca, R. Cingolani, S. Masiero, G. P. Spada and G. Gottarelli, "Photodetectors fabricated from a self-assembly of a deoxyguanosine derivative," *Applied Physics Letters*, vol. 78, no. 22, pp. 3541-3543, 2001.

22. K. H. Yoo, D. H. Ha, J. O. Lee, J. W. Park, J. Kim, J. J. Kim, H. Y. Lee, T. Kawai and H. Y. Choi, "Electrical conduction through poly(dA)-poly(dT) and poly(dG)-poly(dC) DNA molecules," *Physical Review Letters*, vol. 87, no. 19, 2001
23. M. A. Lyshevski, "Multi-valued DNA-based electronic nanodevices," *IEEE Conf. Multi-Valued Logic Design*, Calgary, Canada, 2005.
24. M. Galperin and A. Nitzan, "NEGF-HF method in molecular junction property calculations", *Ann. NY Acad. Sci*., vol, 1006, pp. 48-67, 2003.
25. M. Paulsson, F. Zahid and S. Datta, *Resistance of a Molecule*, *Handbook of Nanoscience, Engineering and Technology*, Ed. W. Goddard, D. Brenner, S. Lyshevski and G. Iafrate, pp. 12.1-12.25, CRC Press, Boca Raton, FL, 2002.
26. Y. Xue, S. Datta and M. A. Ratner, "First-principles based Green's function approach to molecular electronic devices: General formalism," *Chemical Physics*, vol. 281, pp. 154-170, 2002.
27. F. Zahid, M. Paulsson and S. Datta, *Electrical Conduction Through Molecules,* in *Advanced Semiconductors and Organic Nano-Techniques*, Ed. H. Morkoc, Academic Press, NY, 2003.

RECENT PIS PUBLICATIONS DIRECTLY RELATED TO THE PROBLEMS SOLVED

BOOKS (2005):

1. S. E. Lyshevski, *NEMS and MEMS: Fundamentals of Nano- and Microengineering*, CRC Press, Boca Raton, FL, 2005 (second edition).
2. S. Yanushkevich, V. Shmerko and S. E. Lyshevski, *Logic Design of NanoICs*, CRC Press, Boca Raton, FL, 2005.

PAPERS AND PRESENTATIONS (2004-2005):

3. S. E. Lyshevski and T. Renz, "Microtubules and neuronal nanobioelectronics," *Proc. IEEE Conference on Nanotechnology*, Munich, Germany, pp. 379-381, 2004.
4. S. E. Lyshevski and T. Renz, "Three-dimensional molecular electronic architecture and nanoarchitectronics," *Proc. Conf. Fundamentals of Nano*, Salt Lake City, UT, pp. 270, 2005.
5. S. E. Lyshevski and T. Renz, "Carbon-centered quantum nanoelectronics: Novel electronic nanodevices and their analysis," *Proc. Conf. Fundamentals of Nano*, Salt Lake City, UT, pp. 123-127, 2005.
6. S. E. Lyshevski and T. Renz, "Biomolecule-Centered Quantum Nanoelectronics," *NanoBioNICs III*, Marburg, Germany, pp. 47, 2005.
7. M. A. Lyshevski, "Multi-valued DNA-based electronic nanodevices," *IEEE Conf. Multi-Valued Logic Design*, Calgary, Canada, 2005.
8. M. A. Lyshevski, "Design of three-dimensional nanobioelectronics," *Conf. Fundamentals of NANO*, Salt Lake City, NM, pp. 106-110, 2005.
9. M. A. Lyshevski, "Brownian nanobiotransistors: Applied neuronal biomimetics," *Conf. Fundamentals of NANO*, Salt Lake City, NM, pp. 118-122, 2005.
10. M. A. Lyshevski, "DNA electronic nanodevices with application to biomolecular gates," *NanoBioNICs III*, Marburg, Germany, pp. 79, 2005.
11. M. A. Lyshevski, "Brownian dynamics and Brownian nanobioelectronics," *NanoBioNICs III*, Marburg, Germany, pp. 78, 2005.
12. M. A. Lyshevski, "Quantum theory and high-fidelity mathematical modeling of DNA," *Proc. Nanotechnology Conf., IEEE-NANO 2004*, Munich, Germany, pp. 559-561, 2004.
13. M. A. Lyshevski, "Brownian dynamics: Molecular systems modeling and control," *Proc. Nanotechnology Conf., IEEE-NANO 2004*, Munich, Germany, pp. 225-227, 2004.

List of Symbols, Abbreviations, and Acronyms

2D - Two-dimensional

3D - Three-dimensional

ALU - Arithmetic logic unit

BJT - Bipolar junction transistor

CAD - Computer-aided-design

CMOS - Complimentary metal-oxide semiconductor

DD - Decision diagram

DNA^T - DNA transistor

FET - Field-effect transistor

G–V - Conductance-voltage characteristic

HOMO - Highest occupied molecular orbital

ℵ-hypercells - Neuronal hypercell

ICs - Integrated circuit

^{M}ICs - Molecular integrated circuit

I–V - Current-voltage characteristic

^{M}gates - Molecular gate

LDD - Linear decision diagrams

LP - Linear arithmetic polynomial

LUMO - Lowest unoccupied molecular orbital

LWDD - Linear word-level decision diagrams

SLSI - Super-large-scale integration

VLSI - Very-large-scale integration

ULSI - Ultra-large-scale integration